- Technical Paper -

TIME-DEPENDENT DEFORMATIONS OF PVA-ECC UNDER SUSTAINED LOADS: CORRELATION WITH PLASTICITY AND DAMAGE

Benny SURYANTO[*1], Koichi MAEKAWA[*2] and Kohei NAGAI[*3]

ABSTRACT

The evolution of plasticity and fracture under constant, but different stress levels is investigated to study the time-dependent deformations of PVA-ECC under high-stress levels. The elastic deformation in cracked ECC is found to be a good indicator that reflects the rate of plasticity and fracturing. Creep rupture in tension and compression is predicted to occur at stress levels above 75% and at the same order of time exposure in a log scale. From 75% to 90% stress levels, the deformations at rupture are predicted to be 1.1-1.4, and 1.6-3.5 times of those under static tension and compression, respectively.

Keywords: plasticity, damage evolution, creep model, creep rupture

1. INTRODUCTION

Polyvinyl Alcohol Engineered Cementitious Composite (ECC reinforced with randomly distributed short PVA fibers) is a unique cement-based material characterized by a large tensile strain capacity, with the ratio of ultimate tensile strain ε_{tu} to cracking strain ε_{tcr} of 200 or more. It should be noted, however, that the ratio of the corresponding tensile stresses is much smaller and typically in the range of 1.25-1.40. This suggests that tensile stresses that need to be sustained by the material at service loads can be relatively high and hence time-dependent. As cracked state is the intended condition of ECC in use [1], it is essential to investigate its time-dependent behavior in depth.

ECC members undergo time-dependent deformations as a result of drying and/or imposed deformations/loads. This occurs, for instance, in its recent applications as bridge-deck link slabs due to the thermal expansion of adjacent decks, in structural components due to sustained loads, and in retrofit layers due to deformation compatibility. To be serviceable, the time-dependent effects must not be excessive. JSCE [1], for instance, states the time-dependent effects of ECC in tension are deemed to remain acceptably small if tensile creep failure does not occur at the characteristic tensile yield strength.

A common approach to study time-dependent property of a material is by performing creep tests. Although this test is straightforward, it is difficult to perform such tests to develop a thorough understanding for ECC as the testing process can be so much tedious and lengthy. Boshoff and Van Zijl [2] presented the results of tensile creep tests of cracked ECC, but the results were somewhat scatter and inconclusive.

In this paper, a procedure is presented to investigate time-dependent deformations of PVA-ECC under high stress levels with emphasis on the evolution of plasticity and damage. This paper presents the results of specimens under four-point bending and uniaxial compression, describes empirical equations derived from the test specimens, and includes worked examples to demonstrate the usefulness of the test data obtained to form a basis for a wider range of predictions.

2. EVOLUTION OF PLASTICITY AND FRACTURE IN CRACKED PVA-ECC

2.1 Background

The time-dependent responses of cracked PVA-ECC are represented in terms of plasticity evolution and damage progress. The concept proposed by El-Khasif and Maekawa [3] to model the evolution of plasticity and damage of unconfined and confined concrete under uniaxial compression is adapted.

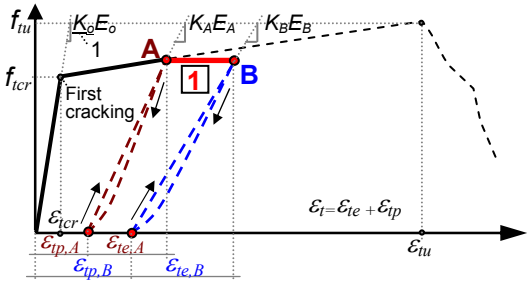

Fig.1 Conceptual illustration

As an illustration, consider the response of a cracked PVA-ECC under tension as shown in Figure 1. Let Points A and B are the start and end of a loading for a time interval *dt*. The change in tensile plastic strain is:

$$\frac{d\varepsilon_{tp,1}}{dt}=\frac{\varepsilon_{tp,B}-\varepsilon_{tp,A}}{dt} \quad (1)$$

*1 Postdoctoral fellow, Dept. of Civil Engineering, The University of Tokyo, PhD, JCI Member
*2 Professor, Dept. of Civil Engineering, The University of Tokyo, Dr. E., JCI Member
*3 Associate Professor, Institute of Industrial Science, The University of Tokyo, Dr. E., JCI Member

where $\varepsilon_{tp,A}$ and $\varepsilon_{tp,B}$ are the tensile plastic strain at States A and B, and can be obtained from rapid stress release from the two states. The average tensile plastic strain can be approximated as:

$$\varepsilon_{tp,1} = \frac{\varepsilon_{tp,A} + \varepsilon_{tp,B}}{2} \tag{2}$$

As the elasticity also changes with time, the average elastic strain can also be approximated as:

$$\varepsilon_{te,1} = \frac{\varepsilon_{te,A} + \varepsilon_{te,B}}{2} \tag{3}$$

The evolving damage is treated in terms of the rate of fracture and the average fracture occurring during the same time interval dt in a similar manner:

$$\frac{dK_{t,1}}{dt} = \frac{K_{t,A} - K_{t,B}}{dt} \tag{4}$$

$$K_{t,1} = \frac{K_{t,A} + K_{t,B}}{2} \tag{5}$$

where K_t is the ratio of stiffness at a time of interest (ie, Point A) to initial stiffness.

2.2 Phenomenological models

This section presents empirical material formulations that were fit to test data of this study. General applicability of the formulations will be examined through their implementation into finite-element algorithms in near future developments.

The normalized plastic strain in cracked ECC is considered as a function of the occurring plasticity rate $d\varepsilon_p/dt$ and the elastic strain ε_e in the following manner:

$$\frac{\varepsilon_p}{\varepsilon_u} = f\left(\frac{d\varepsilon_p}{dt}, \frac{\varepsilon_e}{\varepsilon_u}\right) \cong \frac{a}{\left(\frac{d\varepsilon_p}{dt}\right)^b} \tag{6}$$

where,

$$a = \begin{cases} 2.83\frac{\varepsilon_{te}}{\varepsilon_{tu}} - 0.19\ ;\ a > 0.045 & \textit{for tension} \\ 0.012\exp\left(4\frac{\varepsilon_{ce}}{\varepsilon_{cu}}\right) & \textit{for compression} \end{cases}$$

$$b = \begin{cases} -0.13\frac{\varepsilon_{te}}{\varepsilon_{tu}} + 0.08 & \textit{for tension} \\ 0.2\frac{\varepsilon_{ce}}{\varepsilon_{cu}} + 0.05 & \textit{for compression} \end{cases}$$

a is a damage indicator that primarily controls the accumulated plastic strain ε_p and b is a power term that primarily controls the degree of plastic strain increment, with a and b being a function of the normalized average elastic strain (for tension ε_{te} is normalized with ε_{tu} and for compression ε_{ce} is normalized with the strain corresponding to compressive strength ε_{cu}).

The evolution of fracture K is determined in a similar manner and is as a function of the occurring fracturing rate dK/dt and the average elastic strain ε_e as

$$K = f\left(\frac{dK}{dt}, \frac{\varepsilon_e}{\varepsilon_u}\right) \cong \frac{p}{\left(10000\frac{dK}{dt}\right)^q} + 1 \tag{7}$$

where,

$$p = \begin{cases} -0.11\ln\left(\frac{\varepsilon_{te}}{\varepsilon_{tu}}\right) - 1.0425 & \textit{for tension} \\ -0.7\frac{\varepsilon_{ce}}{\varepsilon_{cu}} + 0.2;\ p > -0.98 & \textit{for compression} \end{cases}$$

$$q = \begin{cases} 0.001\left(\frac{\varepsilon_{te}}{\varepsilon_{tu}}\right)^{-0.7} & \textit{for tension} \\ 0.012\left(\frac{\varepsilon_{ce}}{\varepsilon_{cu}}\right)^{-2.1} + 0.005 & \textit{for compression} \end{cases}$$

p is a damage indicator that mainly controls the degree of fracturing K and q is a power term that controls the degree of fracturing increment, with p and q being a function of the normalized average elastic strain.

3. EXPERIMENTAL PROGRAMS

3.1 Test setup

Fourteen simply-supported specimens, 100×50 mm in cross section and 600 mm in length, were tested under two-point loading conditions. The two point loads were spaced 110 mm apart on the center span and the span length was 500 mm. Table 1 summarizes the details and loading conditions for the specimens tested. All the loads listed in the table are the obtained loads in a percentage of the average static load capacity obtained from Beams B1 to B3 and B11.

Table 1 Beam test specimens

ID	Objective	Load pattern % of capacity (time in seconds)
B1-B3 B11	Static capacity	100% (710, on average)
B10	Cyclic response	71%, 77%, 84%, 86%, 90% 95%, 98%, 98%, 90%
B4	To determine the time-dependent properties of PVA-ECC	68% (275, 369, 606, 602,422) 77% (302, 606, 619, 609, 606, 612, 604, 605), 90%(106)
B5		68% (306, 318, 302) 77% (303, 298, 303) 82% (302, 339), 87% (302,306) 92% (185, 101−CR)
B6		68% (264,244,326,601, 648,601) 80% (305−CR)
B7		70% (1204, 1202, 1205) 79% (185, 1206, 1204, 1207) 88% (308, 305), 93% (63, 44−CR)
B8		82% (183, 605, 1261) 85% (1804, 1806), 100%
B9		72% (616,R), 84% (623,R), 100% (605,R),104% (631,R),108%
B12		59% (606, 1220, 2412) 65% (324, 1706), 100%
B13		55% (602, 1210, 2406, 2528) 70% (612, 1212, 1808, 2352), 96%
B14		58% (332, 604, 604) (all R) 73% (306, 604, 602, 600) 84% (304, 602, 600), 100%

Note: R: under constant displacement, CR: creep rupture.

Table 2 Cylinder test specimens

Specimen number	Objective	Load pattern % of capacity (time in seconds)
C1, C2	Static capacity	100% (365, on average)
C3	To determine the time-dependent properties of PVA-ECC	60% (298, 300, 300) 70% (300, 304, 300) 80% (298, 300, 298) 90% (88, 86, 86), 90%
C4		75% (598, 596) 85% (602, 598), 89%
C5		60% (56), 65% (56) 70% (58), 75% (56) 80% (58), 85% (56) 90% (34), 100%
C6		75% (300, R) 90% (298, R), 100%

Note: R: under constant deformation. Loads are in a fraction of the average compressive strength of Cylinders C1 and C2.

Beams B1 to B3 and B11, taken as the control specimens, were subjected to monotonically increasing displacement-controlled load at a rate of 0.8 mm/min. Beams B4 to B9, B12, and B14 were subjected to cyclic loads, following the load patterns listed in Table 1. The cyclic loading was conducted as follows:

L1. Each of these specimens was initially loaded in a displacement-controlled mode at a rate of 0.8 mm/min until the target load level was achieved.

L2. Loading was then switched to load control to maintain the reaction force to be constant for an intended time span (ie, 10 mins).

L3. Loading was switched to displacement-controlled mode again, allowing the specimen to be unloaded and reloaded again to the same or higher load level. This unloading and reloading process took approximately two minutes.

L4. Loading procedures L2 and L3 were repeated, following the loading patterns shown in Table 1. Failure occurred either due to the applied monotonically increasing displacement or due to creep rupture when the load was held constant.

Six 100×200 mm PVA-ECC cylinders were additionally tested to study the time-dependent nonlinearity in compression. Table 2 summarizes the test program. Two control cylinders were tested under static displacement-controlled loads. The other four cylinders were subjected to cyclic loads, using the same procedure as those adopted for the beam specimens.

3.2 Instrumentation

All beams were instrumented with two LVDTs to measure midspan deflection, two strain gages and two cable transducers (attached to the bottom surface over the constant moment span) to measure surface strains.

The deformations of the cylinders were measured using two LVDTs attached on two aluminum rings spaced 100 mm part at midheight of the cylinder (see Fig. 2). Each ring was connected to the cylinder mechanically at three points.

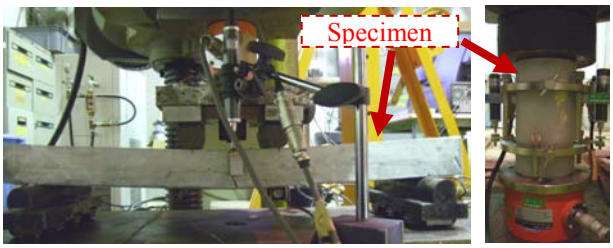

Fig.2 Test setup and instrumentation

3.3 Material and fabrication

A premix PVA-ECC available in Japanese market is used in this study [1]. This premix material contains 2% volume of 12-mm length and 0.04-mm diameter of Polyvinyl Alcohol (PVA) fibers. The mix proportion of this material is shown in Table 3.

Table 3 Mix Proportion of PVA-ECC [1]

W/(C+FA) (%)	Water (kg/m^3)	S/(C+FA) (%)	PVA Fibers (%), in vol.
42.2	350	70	2.0

Note: W: Water, C: Cement, FA: Fly Ash, S: Sand

The PVA-ECC mixture was prepared based on the procedure specified in JSCE Recommendation [1]. For the beam specimens, fresh ECC slurry, after being mixed for ten minutes, was poured into the middle of each steel framework at once and shredded laterally. For the cylinders, the slurry was poured into plastic molds in three layers.

After a day of curing period, all specimens were stripped and then submerged in water in a room with a temperature of 18±3°C until 28 to 34 days of age.

4. TEST RESULTS AND DISCUSSIONS

4.1 Static response

Figure 3 shows the response of Beams B1 to B3 and B11 under static loads. These four beams exhibited a highly ductile behavior, failing in flexure at an average load of 4.68 kN, with a corresponding average midspan displacement of 8.31 mm, and an average tensile strain of 1.74%, measured on the bottom beam surface over the constant moment span.

The average compressive strength of the cylinder specimens was 39.0 MPa and the average strain corresponding to this peak stress was 0.382%.

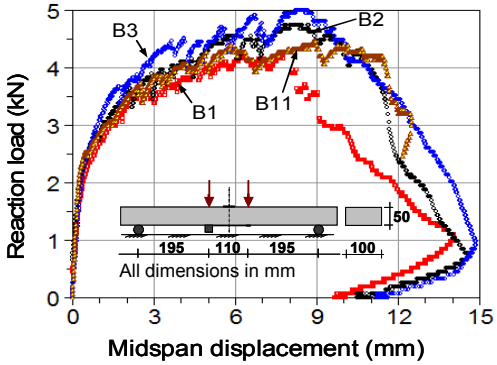

Fig.3 Response of Specimens under static loads

4.2 Cyclic response

A comparison of the load-deformation and deformation-time in flexure and in compression is shown in Figs. 4 and 5, respectively. The loads shown in Fig. 4 are normalized with the average static capacity, while the apparent tensile strains shown in Fig. 5 are the average surface strains measured from each bottom beam surface over the constant moment span.

The test results shown in Figs. 4(a) and (b) indicate that the effects of cyclic and short-term sustained loads on the static capacity and ductility of the beams and the cylinders were minor. Except for Beam B6 that failed prematurely at 80% of its static capacity (the ductility was roughly 50% less), all other specimens were able to sustain at least 90% of their static capacities. No appreciable differences in ductility were evident in all beams tested and slight increase in ductility was observed in the cylinders. Moreover, the test results also indicate that residual deflections and plastic compressive strains were highly irrecoverable and being accumulated through each loading cycle.

As evident from Figs. 5(a) and (b), tensile and compressive strains increased when loading was held constant. The rate of strain increase was more significant when the load level was increased. While the compressive strain under a constant stress always exhibit a gradual increase, the tensile strains sometimes show a sudden increase possibly due to cracking.

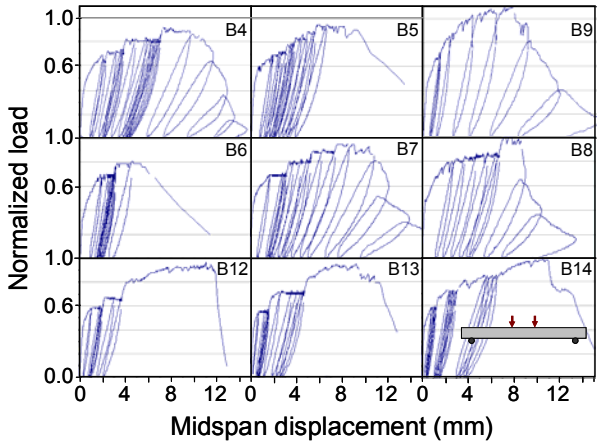

(a) Load-deflection responses under two-point loading

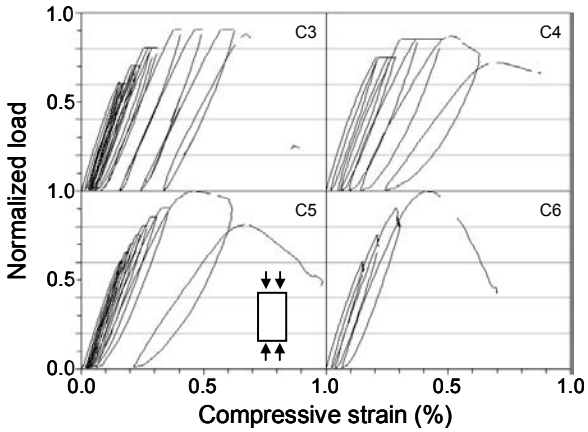

(b) Load-deformation responses under compression

Fig.4 Macroscopic responses under cyclic loads

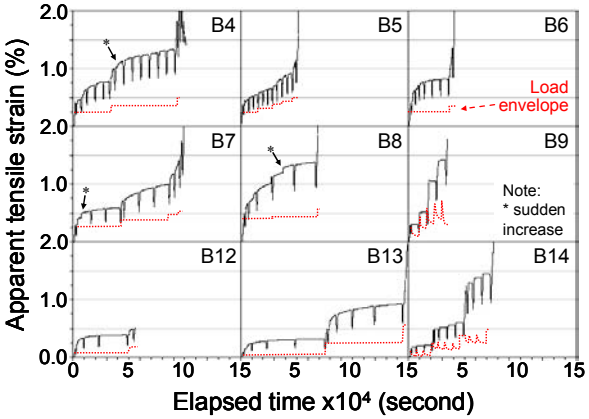

(a) Time-strain responses under two-point loading

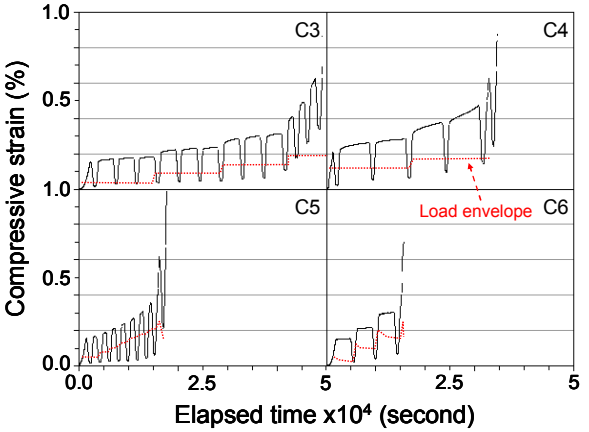

(b) Time-strain responses under compression

Fig.5 Time-strain responses under cyclic loads

With these data at hand, attempts were made to extract the plasticity evolution from the time-deformation responses and to extract the evolving damage from the load-deformation responses. The procedures outlined in Section 2 were used. The results are presented in subsequent sections.

4.3 Evolution of Plasticity and Damage

Figures 6(a) and (b) shows the observed plastic strain rate versus the normalized plastic strain, while Figures 6(c) and (d) shows the observed fracturing rate versus the fracture parameter. The fracturing rates were multiplied by 10^4 to give approximately the same order to the plastic rate (about 0.01 to 100 micron/sec). The markers are the experimental data, the dashed lines represent curve fit obtained from Equations 6 and 7, and the numbers on the line represent the normalized elastic strains. The experimental data having nearly the same magnitude of elastic strain (± 75-100 micron) were grouped together and plotted in the figures using the same markers.

Regarding the rate of plasticity, it is evident from Figs. 6(a) and (b) that the plastic rate increases as the elastic strain increases. The plastic rate decreases as the plastic strain increases. The decrease in plastic rate is more significant in lower elastic strains, as reflected by the milder slope of the curves at lower strain levels. From the same figures, it is also evident that plasticity appears to contribute more to the total deformation in

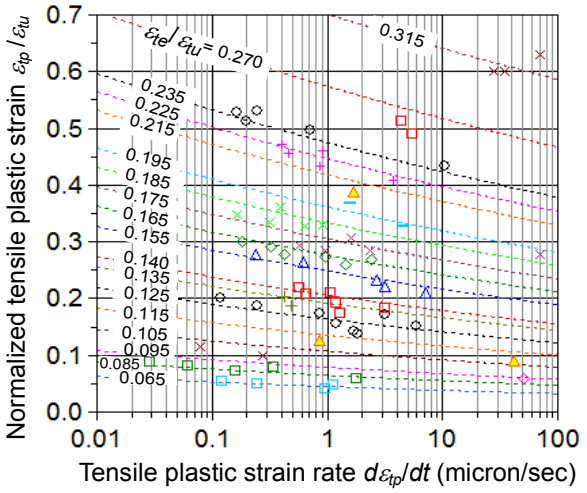

(a) Evolution of plasticity in tension

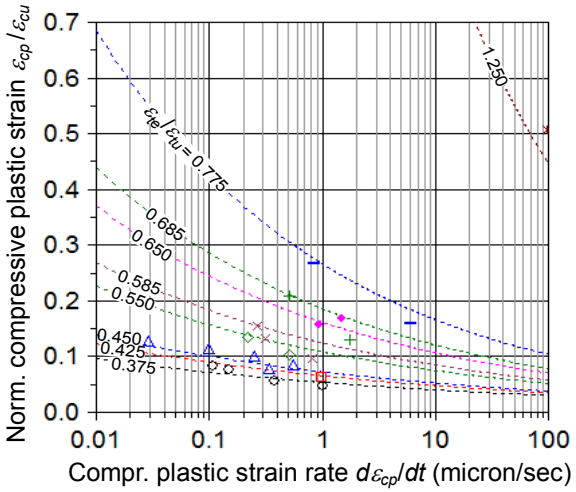

(b) Evolution of Plasticity in compression

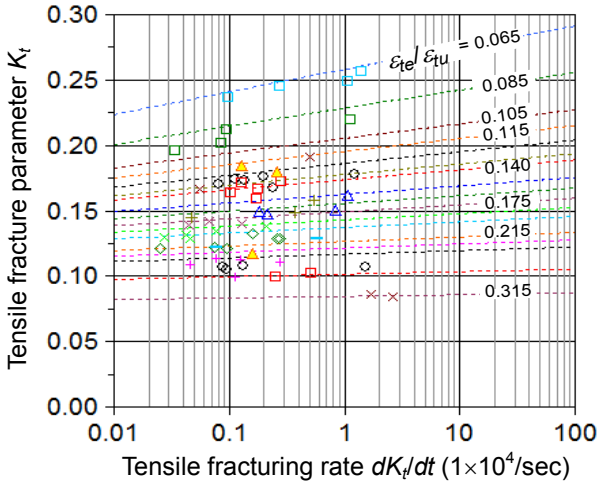

(c) Evolution of fracture in tension

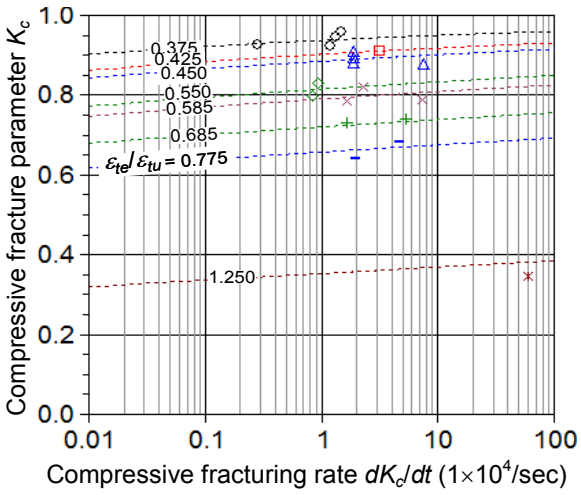

(d) Evolution of fracture in compression

Fig.6 Extracted plasticity and fracture

tension, while elasticity appears to contribute more to the total deformation in compression.

With respect to the rate of fracture, the extracted rate shown in Figs. 6(c) and (d) suggests that as the elastic strain increases the fracturing rate also increases. As the damage increases (fracture parameter decreases), the fracturing rate also decreases.

The fracture parameters K are seen to undergo rapid decrease to less than 0.30 as the specimen tested under two-point loading moved from uncracked to cracked state, while the K values under compression gradually decreases from 0.9 to 0.6.

5. TIME-DEPENDENT DEFORMATIONS—A WORKED EXAMPLE

To demonstrate the use of Equations 6 and 7 proposed, consider five hypothetical PVA-ECC prisms, each subjected to either uniaxial tension or compression at both ends at a stress level of 75%, 80%, and 90% of their static capacity. Table 4 lists the initial normalized strains and fracture parameters that, for under tension, are obtained from the results of Beams B9 (1st load cycle), B8 (1st load cycle), and Beams B10 (5th load cycle) and, for under compression, are obtained from Cylinders C4 (1st load cycle) and C6 (2nd load cycle). Only 75% and 90% stress levels are considered for compression as data for 80% is unavailable.

Table 4 Input variables for prediction

Load level	Tension			Compression		
	$\varepsilon_{te}/\varepsilon_{tu}$	$\varepsilon_{tp}/\varepsilon_{tu}$	K_t	$\varepsilon_{ce}/\varepsilon_{cu}$	$\varepsilon_{cp}/\varepsilon_{cu}$	K_c
75%	0.080	0.082	0.264	0.494	0.052	0.894
80%	0.117	0.154	0.189	—	—	—
90%	0.200	0.288	0.127	0.639	0.142	0.803

Figures 7(a) and (b) shows the computed normalized total strains versus time, while Figure 7(c) shows the corresponding elastic and plastic strains. Creep rupture is analytically distinguished by a rapid increase in total strains as the rate of elastic strain becomes infinitely large, while the rate of plastic strain remains small.

The hypothetical time-dependent responses shown in Figs. 7(a) and (b) indicate that the time corresponding to the occurrence of creep rupture under either tension or compression does not differ significantly. At 75% stress level, they are predicted to occur at the same order of life in a log scale, while at

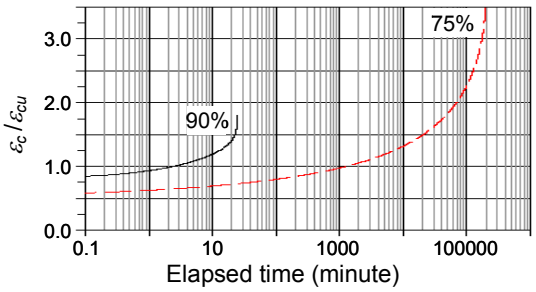

(a) Time-dependent response in compression

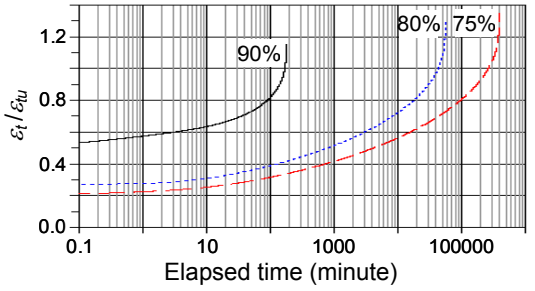

(b) Time-dependent response in tension

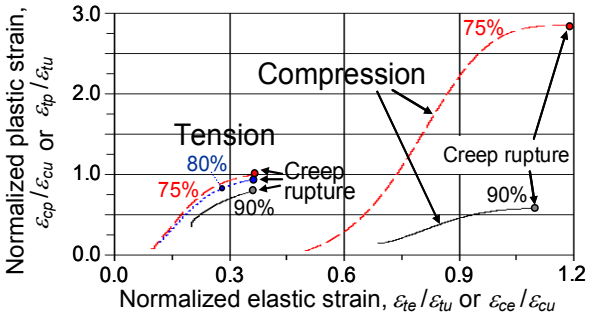

(c) Development of elastic and plastic strains

Fig.7 Hypothetical responses of cracked PVA-ECC under high-level compression or tension

90% stress level the time at rupture in compression is predicted to occur at one order smaller. By contrast, the deformations corresponding to the creep rupture are predicted to be significantly different. While the normalized compressive strains at rupture are predicted to occur in the range of 1.6-3.5 at 75%-90% stress levels, those in tension are between 1.1 and 1.4. The large deformation capacity in compression resembles that of *normal-strength* concrete [4], while that in tension needs to be further validated by experiment.

To explain the difference in the deformation capacity at rupture, the predicted plastic and elastic deformations shown in Fig. 7(c) are discussed. It is evident that the stress level, for the range applied, has a great influence to the proportion of elastic and plastic strains under compression, and has negligible influence to that under tension. At 75% stress level, plasticity is seen to contribute measurably to the compressive deformation capacity, while at 90% stress level elasticity is predicted to contribute more. On the other hand, plasticity is consistently seen to contribute more to the tensile deformation capacity.

From Fig. 7(c), it is also evident that stress level and type of loading do not affect the magnitude of the elastic deformations. The normalized elastic strain capacity is approximately 0.36 and 1.1-1.2, for under tension and compression, respectively.

On the other hand, the type of loading is seen to affect the magnitude of plastic compressive strain. If it is under compression, plastic strain capacity is predicted to increase from 0.58 to 2.85 as the stress level is decreased from 90% to 75%. If it is under tension, they are always comparable and within 0.8 to 1.0. These comparable values might be attributable to the fact that they are limited by crack number and crack width. The difference in the ability of the material to develop this irrecoverable plastic strain explains the difference in the total strain capacity attained.

Finally this paper ends with a note on the rapid increase in elastic deformations at rupture shown in Fig. 7(c) that perhaps best provides a physical explanation to the above description about creep rupture.

6. CONCLUSIONS

(1) Elastic and plastic strains are good indicators to reflect the rate of plasticity in cracked PVA-ECC. As the elastic strain increases, the plastic rate increases. As the plastic strain increases, the plastic rate decreases. The decrease in plastic rate is more significant in lower elastic strains.

(2) Elastic strain does also a good job to reflect the rate of fracture. As the elastic strain increases, the fracturing rate increases. The fracturing rate decreases as the damage increases.

(3) The instantaneous rate of fracture in PVA-ECC under high-level of compression or tension is three to four orders lower than that of plasticity.

(4) Creep rupture is predicted to occur at stress levels above 75% under either compression or tension at a similar order of time period in a log scale. The deformations at rupture under 75%-90% stress levels is 1.1-1.4 (for tension), and 1.6-3.5 (for compression) of the deformation corresponding to the peak stress under static loading conditions.

(5) The difference in deformation capacity is due to the difference in the ability of the material to develop plastic deformation. No significant difference in elastic deformation capacity is observed at stress levels above 75%.

REFERENCES

[1] JSCE, "Recommendations for Design and Construction of HPFRCC with Multiple Fine Cracks," Concrete Library 127, 2007.

[2] Boshoff, W. P., Mechtcherine, V., and van Zijl, G. P. A. G., "Characterizing the Time-dependent Behaviour on the Single Fibre Level," Cement and Concr. Research, Vol. 39, 2009, pp. 779-786.

[3] El-Khasif, K. F., and Maekawa, K., "Time-dependent Nonlinearity of Compression Softening in Concrete," J. of Advanced Concrete Technology, Vol. 2, No. 2, 2004, pp. 233-247.

[4] Rusch, H., "Research towards a General Flexural Theory for Structural Concrete," Proc. of ACI, Vol. 57, 1960, pp. 1-28.